

# Advances in laboratory modeling of wave propagation

Thomas E. Blum\* and Kasper van Wijk, Boise State University

## SUMMARY

Laboratory studies of ultrasonic wave propagation can serve as either scaled modeling of challenges in seismic imaging, or as a way to investigate fundamental advancements in wave propagation. Particularly non-contacting laser ultrasonics provides tremendous opportunities toward both mentioned purposes, because the laser acquisition allows for automated scanning, a small source/receiver footprint and does not suffer mechanical ringing of traditional contacting ultrasonic sensor. Here we present calibration measurements of a new two-component laser receiver, as well a novel way of scaled modeling with structures made in glass.

## INTRODUCTION

Studies of elastic wave propagation in the laboratory fits in between theoretical and numerical methods on the one hand, and field-scale (seismic) experiments. Laboratory data has the real-life problems of noise, but has the advantage of doing controlled experiments. Traditionally, contacting piezoelectric transducers have been used as both source and receiver in ultrasonic laboratory studies. However, using these introduces mechanical ringing and variations in coupling. In addition, transducer size is on the order of the resonant wavelength, which can make them scatter the wavefield. Laser-based ultrasound has become an alternative non-contacting technique to traditional contacting transducers (Scruby and Drain, 1990). Ultrasonic laser interferometers and vibrometers have a broadband response and a sub-millimeter spot size. Since laser-based sensors do not require physical coupling, one can scan a surface under computer control. Additionally, laser-based sensors are able to output the absolute displacement or velocity of the sample surface, depending on the sensor design.

Based on these advantages, laboratory-scale experiments using laser-based ultrasounds are providing an optimal way to study wave propagation in inhomogeneous media and to mimic seismic experiments in the lab (Nishizawa et al., 1997; Scales and Malcolm, 2003). They offer broadband generation and detection, allow for “surveys” with hundreds of sources and receivers, and, just like geophones in the field, laser sensors’ receiver size is negligible with respect to the wavelengths of interest. Here, we present a new sensor and an application demonstrating the advantages and potential of a new, two-component, non-contacting laser ultrasonics laboratory system.

## MULTICOMPONENT DETECTION

Together with Bossa Nova Technologies, we developed a new two-component (vertical and radial) laser ultrasonic sensor. Here we calibrate our two-component sensor using a Rayleigh

wave, and demonstrate how this sensor allows for fast two-component scanning of the ultrasonic wavefield. With this sensor, we keep pace with the (exploration) seismic community in recording and analyzing more than just the vertical component of the wavefield.

Our sensor is a new prototype of a multi-component laser interferometer, based on an existing out-of-plane receiver. It uses a constant-wave doubled Nd:YAG laser, generating a stable 250 mW beam at a wavelength of 532 nm. The beam is split into a probe beam which is reflected by the sample surface and a reference beam which follows a fixed optical path inside the device. The receiver uses Two-Wave Mixing (TWM) in a photo-refractive crystal to deliver the true displacement of the sample surface. A known displacement at a low frequency is introduced on the reference beam and allows for absolute measurements of the ultrasonic displacements. We take advantage of the roughness of the material surface by collecting the light scattered away from the angle of incidence, which carries information on the in-plane displacement. The collected light is then imaged on a linear photodiode array and the in- and out-of-plane signals are processed electronically. The sensor has a 10 kHz – 10 MHz bandwidth.

## Point measurement

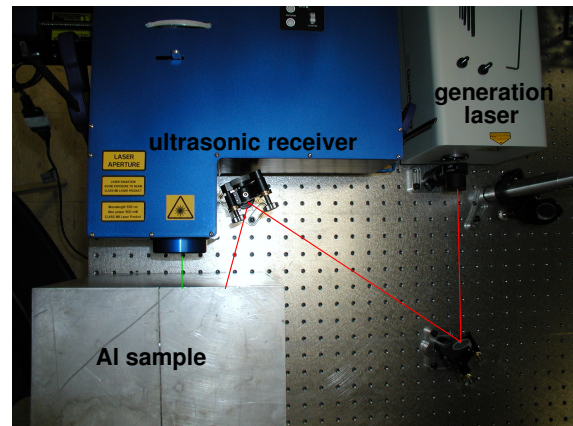


Figure 1: Top view of the experimental setup with the generation beam marked in red and the receiver beam in green. In-plane motion is along the horizontal axis in the figure, and out-of-plane motion is along the laser receiver beam (vertical in the figure).

We measure the amplitude and phase of a Rayleigh wave in an aluminum block (214x232x277 mm) previously described in Scales and van Wijk (1999, 2001); van Wijk et al. (2004a,b). The source spot is approximately 4 mm in diameter and is located 77 mm from the receiver (Figure 1). The in- and out-of-plane signal are averaged 500 times and then band-pass filtered between 300 and 900 kHz, so that all edges of the sam-

## Laboratory wave propagation

ple are tens of wavelengths away. The Rayleigh wave in this effectively homogeneous isotropic half-space is characterized by elliptical retrograde motion at the free surface: the horizontal and vertical components of the displacement are  $90^\circ$  out of phase. Furthermore, the ratio between the maximum amplitudes of the two components (the so-called H/Z ratio) is  $2\sqrt{1 - c_x^2/\beta^2} / (2 - c_x^2/\beta^2)$ , where  $\beta$  is the shear wave velocity and  $c_x$  the Rayleigh wave velocity (Malischewsky and Scherbaum, 2004; Stein and Wysession, 2002). The sample is considered non-dispersive for this application. Based on our data and previous studies using this sample,  $\alpha = 6060$  m/s,  $\beta = 3120$  m/s and  $c_x = 2905$  m/s, resulting in an H/Z ratio of 0.64.

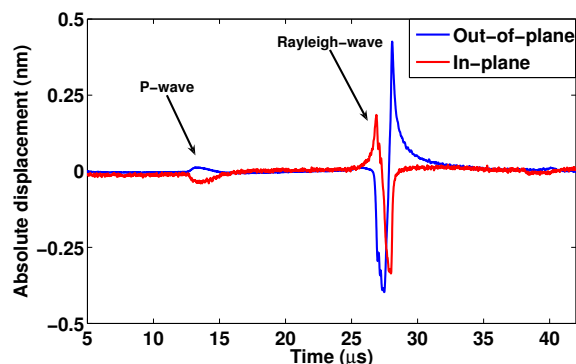


Figure 2: Unfiltered signal recorded by the interferometer 77 mm away from the source. Positive values are radially outward and up.

The absolute displacements from both channels are presented in Figure 2. We compute the H/Z ratio from the discrete amplitudes in the power spectrum and obtain the phase difference by subtracting the unwrapped phase angles of the complex part of the Fourier transform. The H/Z ratio is  $0.64 \pm 0.02$ . However, we find the phase difference between the in- and out-of-plane wavefields to be  $97 \pm 1^\circ$ , a bias of  $7^\circ$ . All error bars represent the uncertainty at  $2\sigma$ , where  $\sigma$  is the standard deviation in the phase and amplitude calculation over all frequencies, respectively. This phase offset originates from a difference in the frequency response between the electronic circuitry for calculation of the in-plane and out-of-plane signals. In the future, the phase difference can be eliminated by carefully matching the frequency response of both in-plane and out-of-plane circuits.

### A line scan

We place the receiver on a motorized stage to record the ultrasonic signals at source-detector offsets between 74 and 101 mm, acquired every half millimeter (Figure 3). The acquisition is fully automated and under computer control. Once we focus the beam in the center of the acquisition line, the entire scan is automatic and lasts on the order of minutes. Figure 4 displays an average H/Z ratio of  $0.63 \pm 0.05$ , and a phase difference of  $100 \pm 4^\circ$ . We attribute variations in the scan results to small variations in detector focus, caused by variable distance to the sample on the order of tens of  $\mu\text{m}$ . Because a large collecting angle is required for good in-plane sensitivity, it is

critical to be well positioned at the focus in order to achieve accurate in-plane measurement. Future work will involve the development of an auto-focusing module in order to maintain the focus position corresponding to the lowest in-plane noise level and obtain the highest accuracy in phase and amplitude in automated scans.

## SCALED MODELING

Laboratory-scale seismology experiments are optimally positioned between full-scale field measurements and theory/numerical simulations. Laboratory experiments create a controlled situation but include real-life issues such as noise and geometry restrictions. Moreover, the sample can be chosen to simulate typical field characteristics, such as fractures, anisotropy or variable porosity in layers.

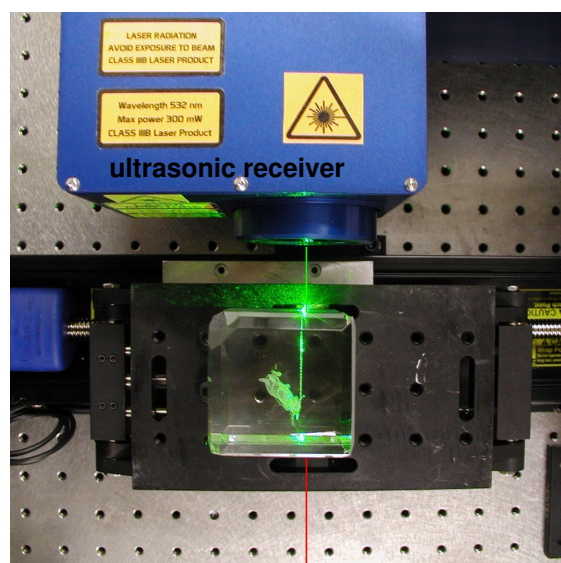


Figure 5: Top view of the experimental setup with the generation beam marked in red and the receiver beam in green. The mule glass cube is fixed to a mechanical stage and displaced along the horizontal axis perpendicular to the laser beams.

Here we present P-wave transmission data through a  $62 \times 62 \times 62$  mm glass cube. Within the sample, bubbles are engraved with the shape of a mule (coincidentally the mascot of Colorado School of Mines). We generate on-axis P-waves with a pulsed high-energy Nd:YAG laser source with a 20 Hz repetition rate. The source beam is partially focused, resulting in a circular source spot approximately 6 mm in diameter. The detection is done on-axis with our laser sensor on the opposite side of the cube. The glass sample is fixed on a computer-controlled mechanical stage, allowing us to scan across the sample along the horizontal axis. We acquire and stack 500 shots for each location, resulting in 72 traces with 0.5 mm offset. A picture of the experimental setup is shown in Figure 5. In order to get a sufficient amount of light scattered back inside the sensor we adhere reflective tape on the receiver side of the glass sample. The signal is acquired on

### Laboratory wave propagation

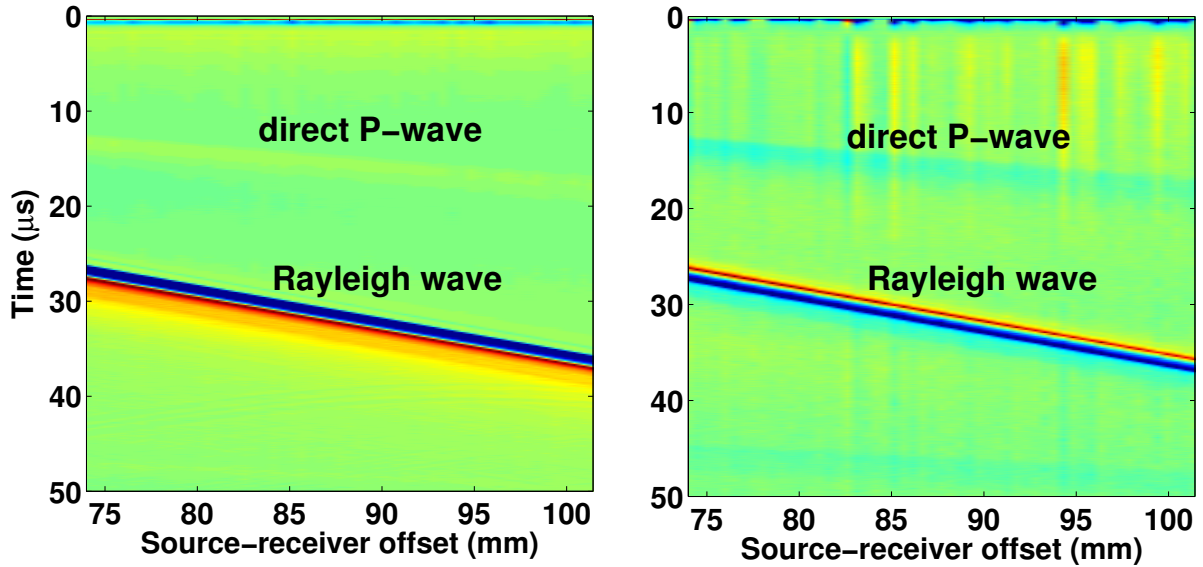


Figure 3: Line scan for the out-of-plane component (left), and the in-plane component (right).

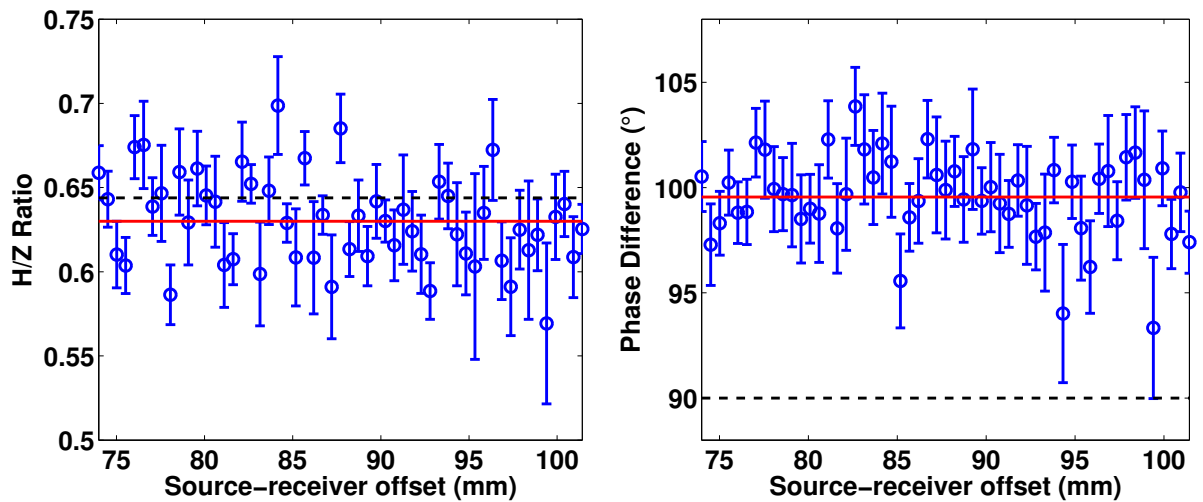


Figure 4: Amplitude ratio (left) and phase difference (right) as a function of source-detector offset. The average and theoretical values are plotted in red (solid line) and black (dashed line), respectively.

## Laboratory wave propagation

a two-channel computer oscilloscope board with a sampling frequency of 100 MS/s and a resolution of 16 bits.

The generated P-wave has a center frequency around 1.5 MHz. The glass has a P-wave velocity  $\alpha \approx 5200$  m/s, leading to a wavelength  $\lambda \approx 3.7$  mm. We assume the tape to be no thicker than  $200 \mu\text{m}$  and therefore neglect its influence on the wave propagation. Bubble radius is estimated to be on the order of one millimeter, and therefore barely resolvable. After applying a 100 kHz – 3 MHz bandpass filter to the data, most of the traces in the 2D scan show a consistent first arrival at  $t \approx 12 \mu\text{s}$ . However traces for which the direction of propagation goes through the body of the mule — and thus the bulk of the bubbles — exhibit a P-wave arrival time lag, representing about 3% of the total travel-time. We interpret this as a slow-down due to the high density of bubbles. The results overlaid by a picture of the sample are presented in Figure 6.

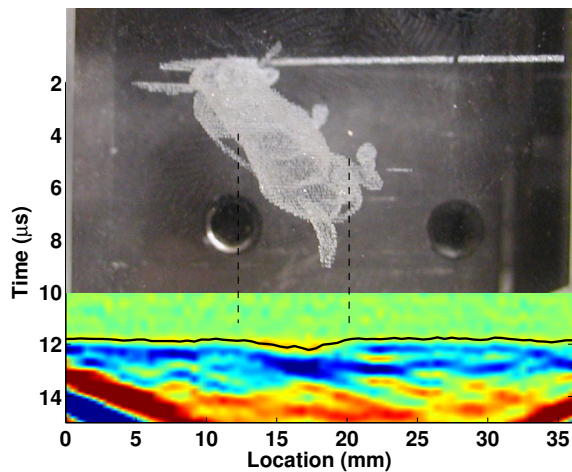


Figure 6: Transmission scan with the P-wave arrival marked by a black line, overlaid by a picture of the sample. As the bubble engraved drawing is leaning down, the scan intersects the bubbles at the middle of the mule shape only.

These preliminary results are promising and show the potential to study geologic features such as salt domes, reservoirs or fracture networks by creating custom-made glass models to use in the laboratory. Future work includes reflection experiments on samples that simulate challenging geological configurations and validation of numerical experiments, such as imaging structures using multiply scattered waves (Malcolm et al., 2009).

## CONCLUSION

Ultrasonic laboratory scale modeling can offer a crucial link between theory and numerical modeling experiments on the one hand and real field experiments, on the other. Particularly, now we have introduced models that can be designed to reflect structures of interest to the seismologists. Piezoelectric transducers, with center frequency 2.25 MHz (slightly higher than our system), have a typical footprint size of 10 to 20

mm and tend to average the wavefield over many wavelengths. Conversely, our laser system has a footprint on the order of millimeters, therefore we more accurately record the wavefield. To keep pace with current practices of multi-component data acquisition, we introduce a new two-component laser receiver. This means we can record multi-component 3D non-contacting mini-seismic surveys, under full computer control.

## ACKNOWLEDGMENTS

Funding for the development of the two-component sensor was provided by the NSF under grant #IIP-0712620. We thank Bruno Pouet, Nicolas Lefaudeux and Alexis Wartelle from Bossa Nova Technologies for the development of the sensor. We also thank Dylan Mikesell, Roel Snieder and Deborah Fagan for useful discussions and comments.

## Laboratory wave propagation

### REFERENCES

- Malcolm, A. E., B. Ursin, and M. V. de Hoop, 2009, Seismic imaging and illumination with internal multiples.: *Geophysical Journal International*, **176**, 847–864.
- Malischewsky, P. G., and F. Scherbaum, 2004, Love's formula and H/V-ratio (ellipticity) of rayleigh waves: *Wave Motion*, **40**, 57–67.
- Nishizawa, O., T. Satoh, X. Lei, and Y. Kuwahara, 1997, Laboratory studies of seismic wave propagation in inhomogeneous media using a laser doppler vibrometer: *Bulletin of the Seismological Society of America*, **87**, 809–823.
- Scales, J. A., and A. E. Malcolm, 2003, Laser characterization of ultrasonic wave propagation in random media: *Physical Review E*, **67**, 046618.
- Scales, J. A., and K. van Wijk, 1999, Multiple scattering attenuation and anisotropy of ultrasonic surface waves: *Applied Physics Letters*, **74**, 3899–3901.
- , 2001, Tunable multiple-scattering system: *Applied Physics Letters*, **79**, 2294–2296.
- Scruby, C., and L. Drain, 1990, *Laser Ultrasonics Techniques and Applications*, 1 ed.: Taylor & Francis.
- Stein, S., and M. Wysession, 2002, *An introduction to seismology, earthquakes and earth structure*, 1 ed.: Wiley-Blackwell.
- van Wijk, K., M. Haney, and J. A. Scales, 2004a, 1D energy transport in a strongly scattering laboratory model: *Physical Review E*, **69**, no. 3.
- van Wijk, K., D. Komatitsch, J. A. Scales, and J. Tromp, 2004b, Analysis of strong scattering at the micro-scale: *Journal of the Acoustical Society of America*, **115**, no. 3.